Progress In Electromagnetics Research M, Vol. 112, 191–203, 2022

InGaAs HEMT Broadband Microstrip Resistive-Terminated Low Noise Amplifier

Moustapha El Bakkali*, Hanae Elftouh, Naima Amar Touhami, Imane Badaoui, and Lamsalli Mohammed

Abstract—This paper presents the design, co-simulation, and measurement of a two-stage broadband-cascaded low noise amplifier (LNA) using resistive terminated architecture. This architecture extends the bandwidth of a low-noise amplifier while maintaining a low NF and high flat gain S_{21}. The LNA is designed with planar technology and mounted on an FR4 substrate. The used InGaAs HEMT MGF4918D transistor from Mitsubishi technology has very low noise and operates up to 18 GHz. The reflection coefficient results of the studied LNA are lower than -10 dB. The stability is unconditional over the entire operating band. The measured gain is $14\,\text{dB} \pm 0.75\,\text{dB}$ with a minimum NF noise figure of 2.9 ± 0.4 dB. The group delay is 0.605 ± 0.145 ns. The 1 dB compression point is 10.16 dBm, and the third order input intercept point IIP3 is 14.25 dBm. Two-stage cascaded LNA has a total power consumption of 164 mW and occupies an area of $7 \times 1.3\,\text{cm}^2$.

1. INTRODUCTION

The problem with wireless communications systems is that the frequency spectrum reaches its occupancy limit. Broadband systems have been utilized to solve many transmission problems. The capacity of a broadband system will be greater than that of a narrowband system [1, 2]. Broadband transmission has several advantages, and the most important ones are bandwidth, improved transmission channel capacity, and high temporal accuracy for geolocation systems [3–6].

Low noise amplifiers, or LNAs, are active, low nonlinear devices frequently used in RF and microwave radio frequency circuits, such as wireless communication systems (cellular phones, radio communication networks, satellite communication, broadcasting) [7–9], medical imaging systems [10, 11], and military radars [12, 13].

The design of a wideband LNA is more complex than that of a narrowband LNA. Matching networks must be designed to ensure nearly invariable gain with minimal noise figure, but this can be very difficult due to the frequency dependence of the transistor S-parameters. The resistive feedback architecture makes it possible to widen the bandwidth except that it brings back the output noise at the input with high DC consumption [14]. The $1/g_m$ termination architecture is matched to the transistor's gm transconductance, which limits the degree of linearity and power consumption [15]. It also has a noise figure of more than 3 dB which is too large for some applications. The resistance-terminated architecture provides $50\,\Omega$ input impedance matching through a resistor, which makes the recovered power maximum, and the resulting thermal noise can contribute to the noise figure degradation of this amplifier [16].

The current problem with broadband LNAs in planar technology is their difficulty in matching the input with a reduced number of LC resonators or microstrip lines and having a low noise level over

Received 26 April 2022, Accepted 21 July 2022, Scheduled 7 August 2022

* Corresponding author: Moustapha El Bakkali (Moustapha.elbakkali@etu.uae.ac.ma).

The authors are with the Laboratory of Information System and Telecommunication, Department of Physics, Faculty of Sciences, Abdelmalek Essaadi University, BP.2121 M'Hannech II, Tetouan 93030, Morocco.

the entire band. Indeed, the ideal source impedance for the minimum noise added by the transistor varies with the frequency. In addition, ohmic losses in the passive components of the circuit contribute to the noise, which is determined in part by the losses of the interconnecting metal element in a given technology.

This paper aims to solve the problem of matching the input of LNA for a total transmission of radio frequency (RF) power with minimal noise figure. Broadband LNA in planar technology proposed is based on resistive-termination technique and has high flat gain, minimum noise figure, high linearity, miniaturized size, low cost and reasonable DC consumption.

2. LNA THEORY

2.1. Select of Active Component

The choice of transistor plays a crucial role in the design of LNAs; the transistor MGF4918D is characterized by small size as shown in Fig. 1(a), minimal noise figure NF, and provides high gain S_{21}. NF and S_{21} are parameters that will be studied in the coming section. The small-signal model of the HEMT is shown in Fig. 1(b).

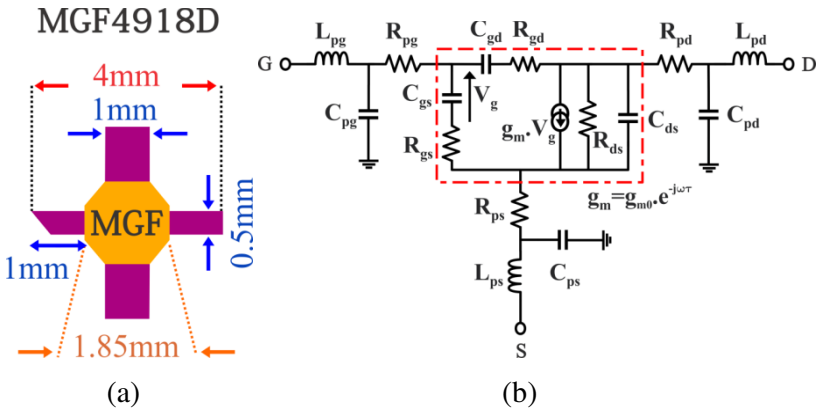

Figure 1. (a) Layout dimensions and (b) small signal equivalent schematic of the MGF4918D transistor.

2.2. Noise Figure NF

The noise picked up by the antenna and the noise generated by active and passive components influence wireless communication systems. It breaks down into noise of artificial origin (electric motors, illuminated signs, ...) and noise of natural origin (noise from the earth, noise from the atmosphere, ...).

The noise figure in the presence of an admittance source Y_s is given by [17]:

$$\mathrm{NF} = \mathrm{NF}_{\min} + \frac{R_n}{\mathrm{Real}\,(Y_s)}\,|Y_s - Y_{\mathrm{opt}}|^2 \tag{1}$$

- R_n: The empirical constant is linked to the noise factor's sensitivity to the generator's admittance with a dimension of resistance.
- Y_{opt}: Admittance of the source, which gives a minimum noise figure.
- The minimum noise figure $\mathrm{NF}_{\min}$ is given by an empirical Fukui equation [18]:

$$\mathrm{NF}_{\min}\ (\mathrm{dB}) = 10\log\left(1 + 2\pi K_0 f C_{gs}\sqrt{\frac{(R_{ps}+R_{pg})}{g_m}}\right) \tag{2}$$

- K: A factor linked to the quality of the material of the canal.
- C_{gs}: The grid-source capacity.
- R_{ps} and R_{pg}: Extrinsic source and gate resistance.
- f: The operating frequency.

2.3. Gain S_{21}

One of the key reasons for situating the amplifier at the reception chain's input is to reduce the noise in subsequent stages, as justified by Friiz's equation [19]. As a result, adequate amplifier gain is also necessary. The overall gain of a multi-stage amplifier is determined by the gain of each stage and the load on each stage. The gain is linked to power transmission and therefore to impedance matching.

The expression of gain S_{21} for the intrinsic part of the transistor mounted as a common source is:

$$S_{21} = \frac{2\dfrac{-g_m}{1+jR_{gs}C_{gs}\omega} + j\omega C_{gd}}{1 + \dfrac{1}{R_{gs} + \dfrac{1}{j\omega C_{gs}}} + j\omega C_{gd} + j\omega\left(C_{ds}+C_{gd}\right) + \dfrac{1}{R_{ds}} + \Delta Y} \tag{3}$$

where:

$$\Delta Y = \left(\frac{1}{R_{gs} + \dfrac{1}{j\omega C_{gs}}} + j\omega C_{gd}\right)\left(j\omega\left(C_{ds}+C_{gd}\right) + \frac{1}{R_{ds}}\right) - j\omega C_{gd}\left(\frac{-g_m}{1+jR_{gs}C_{gs}\omega} + j\omega C_{gd}\right)$$

2.4. Linear Stability Study

The stability of a transistor is its resistance to oscillation in the frequency band studied.

The study of the stability of an amplifier is important for avoiding any oscillation of the stage, which could cause it to malfunction. The analysis of the stability of a transistor is an essential point for the design of an amplifier. Indeed, the correct operation of a circuit can be disturbed by oscillations.

2.4.1. Rollet Factor K

The study of linear stability is carried out from an analysis of scattering parameters of LNA. The Rollet factor K method successively charges the input and output of the quadrupole with a passive impedance having the modulus of its reflection coefficient less than unity. This criterion leads to the following unconditional stability [20].

$$k = \frac{1 - |S_{11}|^2 - |S_{22}|^2 + |\Delta|^2}{2\,|S_{12}S_{21}|} > 1 \tag{4}$$

$$|\Delta| < 1 \tag{5}$$

where $\Delta = S_{11} \cdot S_{22} - S_{12} \cdot S_{21}$.

2.4.2. Stability Factor

Based on the two equations (4) and (5) and the circles of stability, we define a new stability criterion denoted as μ_1 and μ_2 and defined by the following equations [21]:

$$\mu_1 = \frac{\left(1 - |S_{22}|^2\right)}{\left(|S_{11} - S_{22}^* \cdot \Delta| + |S_{12} \cdot S_{21}|\right)} > 1 \tag{6}$$

$$\mu_2 = \frac{\left(1 - |S_{11}|^2\right)}{\left(|S_{22} - S_{11}^* \cdot \Delta| + |S_{12} \cdot S_{21}|\right)} > 1 \tag{7}$$

μ_1 and μ_2 specify the distance between the Smith chart center and the nearest unstable-input (source μ_1) and output (load μ_2) circles stability. The single necessary and sufficient condition for the 2-port network's unconditional stability is that $\mu_1 > 1$ or $\mu_2 > 1$.

2.5. LNA Linearity

Several phenomena contribute to the appearance of distortions that affect low noise amplifiers. One of the major causes of active element non-linearity is gain compression. We denote $P_{1\,\mathrm{dB}}$ as the compression point where the gain has dropped by 1 dB compared to its nominal value. The other one is third order intermodulation (IP3) distortion, which is a measure of the effect of harmonics in a system [22]. This is the power to which the fundamentals and the products of order 3 are equal. Under the condition that the power gain (dB) is equal to S_{21} (dB), the IIP3s are calculated according to the following equation.

$$\mathrm{IIP3\ (dB)} = \mathrm{OIP3\ (dB)} - S_{21}\ \mathrm{(dB)} = \mathrm{OP}_{1\,\mathrm{dB}} + 9.64\ \mathrm{(dB)} - S_{21}\ \mathrm{(dB)} \tag{8}$$

OIP3 is the 3rd order output intermodulation point, and $\mathrm{OP}_{1\,\mathrm{dB}}$ is the output compression point.

2.6. Group Delay

Group delay, or GD, is a critical parameter in designing low-noise amplifiers applied to broadband and UWB wireless telecommunication systems [23]. Indeed, GD translates the delay of the signal as a function of the frequency, which might result in an incorrect measurement, while its high fluctuation results from impulsion distortions that complicate the measurement or compromise the signal's integrity.

GD is defined as the variation of the phase ϕ with respect to the pulsation ω [24]:

$$\mathrm{GD} = -\frac{\mathrm{d}\varphi\,(S_{21})}{\mathrm{d}\omega} = -\frac{1}{2\pi}\cdot\frac{\mathrm{d}\varphi\,(S_{21})}{\mathrm{d}f} = -\frac{1}{360^\circ}\cdot\frac{\mathrm{d}\theta\,(S_{21})}{\mathrm{d}f} \tag{9}$$

φ: in radians; ω: in radians/sec; θ: in degrees; f: in Hz ($\omega = 2\pi f$).

2.7. Factor of Merit FOM

In the literature, the factor of merit FOM is used to compare the design quality of LNAs in different technologies and applications. The expression of FOM for broadband LNAs is [25]:

$$\mathrm{FOM} = \frac{G_{\mathrm{abs}}\cdot \mathrm{IIP3\ (mW)}\cdot \mathrm{BW\ (GHz)}}{(\mathrm{NF}-1)_{\mathrm{abs}}\cdot P_{\mathrm{dc}}\ \mathrm{(mW)}} \tag{10}$$

where:

G: Gain S_{21}; IIP3: third-order input intercept point; BW: bandwidth; NF: Noise figure; and P_{dc}: dissipated power.

3. STUDY OF THE PROPOSED ARCHITECTURE OF BROADBAND LNA

3.1. Schematic of the Proposed Broadband LNA

The cascaded broadband LNA in Fig. 2 consists of two stages. The input adaptation to have a total power transmission and a minimum noise is very complex. The proposed solution is to perform the

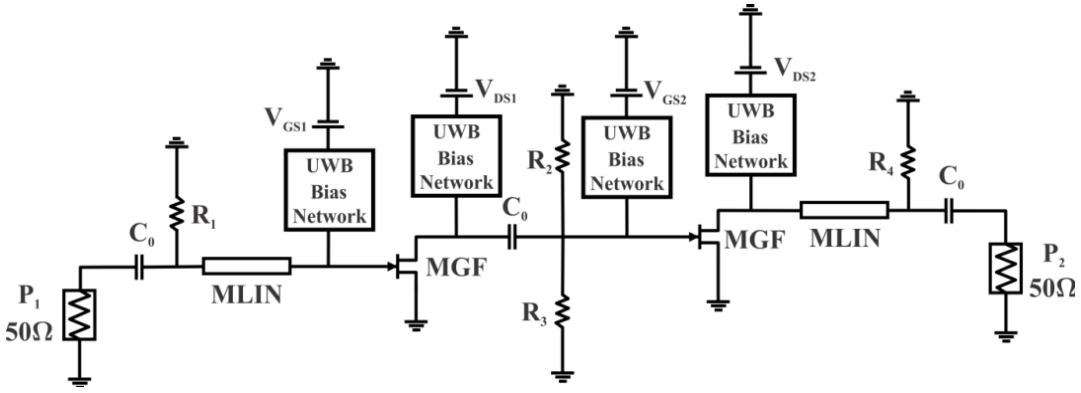

Figure 2. Complete schematic of the proposed cascaded broadband LNA.

matching with a minimal number of resistors. Resistor R_1 with the MLIN line provides matching of S_{11} close to -7 dB with a minimum noise figure. R_2 and R_3 are placed at the input of the second stage to improve the performance of LNA (Minimization of gain and noise ripple) over the entire operating band. R_4 with the MLIN line guarantees the total power transmission to the load. R_4 with the MLIN line guarantees the total power transmission to the load. C_0 capacitors are used to block the passage of the DC component.

3.2. Design of Broadband Bias Tee Network

Figure 3 shows the proposed broadband bias Tee-network. It consists of the main RF line of a length of 3.6 mm. Shunt capacitor C_b is used to circuit the leakage of the RF signals to port P_3. Two radial bypass lines are used to solve the bandwidth expansion problem of the bias T-network.

The bias T-network is mounted on an FR4 substrate, whose properties are shown in Table 1.

Table 1. Properties of the FR4 substrate.

ε_r	H (mm)	T (µm)	Tanδ
4.3	0.6	35	0.02

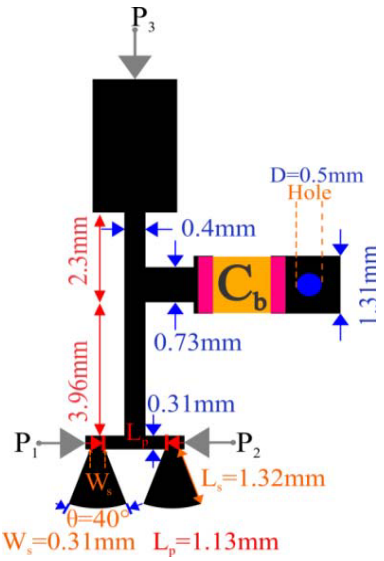

Figure 3. Broadband bias network proposed.

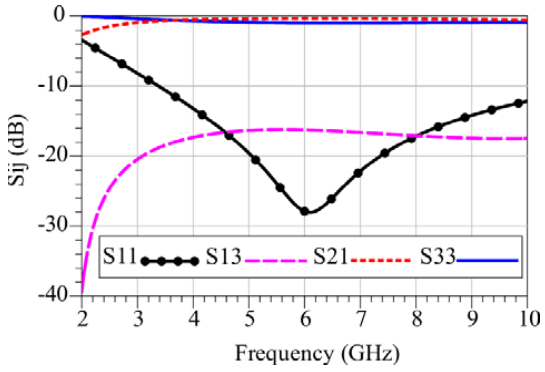

Figure 4. S-parameters results of bias Tee network.

Figure 4 shows the results of the simulation of the polarization tee array. The reflection coefficient S_{11} at port P_1 is less than -10 dB. The isolation S_{13} between P_1 and P_3 is perfect (< -16 dB). The reflection coefficient S_{33} at P_3 is total, which means that the RF signal does not pass through this port but only follows the path from P_1 to P_2, as shown by the transmission coefficient S_{21}, which tends to 0 dB.

3.3. Bias Effect on NF and Gain S_{21}

Figure 5 shows the evolution of NF, with S_{21} as a function of the voltage V_{GS}. NF takes a minimum value for V_{GS} lower than -0.3 V. The gain S_{21} is flat over the frequency band. It increases with V_{GS} and saturates at a value of -0.1 V. The optimal value of V_{GS} is therefore -0.1 V. In Fig. 6, drain-source voltage V_{DS1} of the first stage influences the noise figure NF, especially in the 3 GHz and 6 GHz bands.

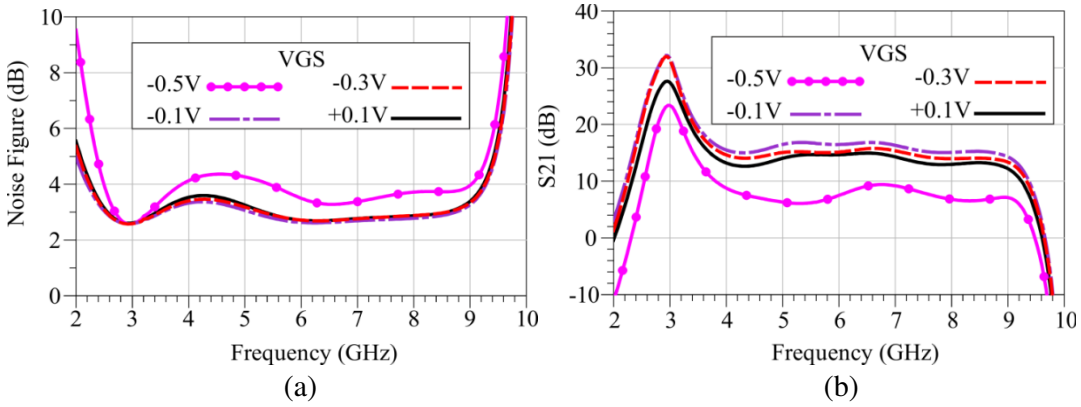

Figure 5. (a) Noise figure NF and (b) forward gain S_{21} for several values of gate-source voltage V_{GS} ($V_{DS1} = 0.8\,\text{V}$ & $V_{DS2} = 0.8\,\text{V}$).

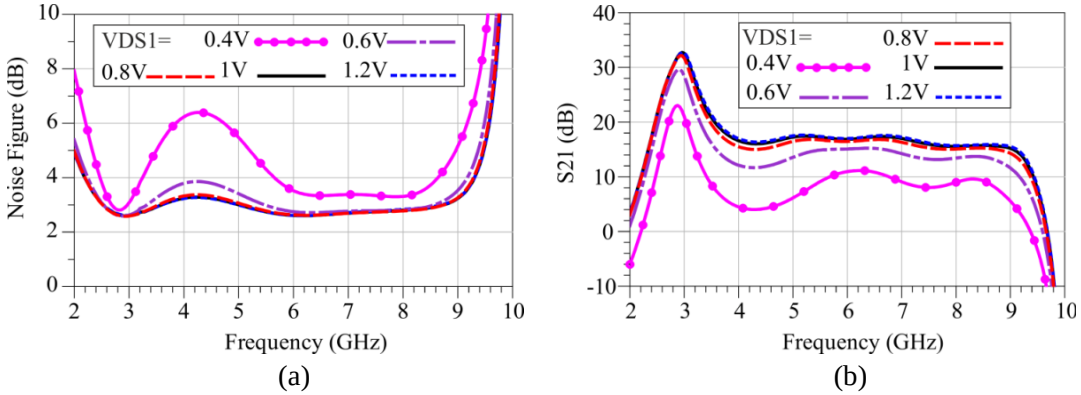

Figure 6. (a) Noise figure NF and (b) forward gain S_{21} for several values of drain-source voltage V_{DS1} of the first stage ($V_{GS} = -0.1\,\text{V}$ & $V_{DS2} = 0.8\,\text{V}$).

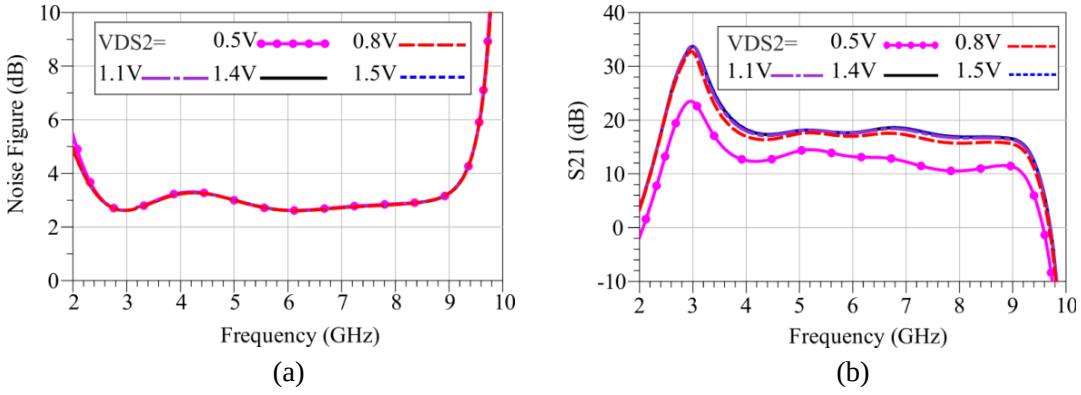

Figure 7. (a) Noise figure NF and (b) forward gain S_{21} for several values of drain-source voltage V_{DS2} of the second stage ($V_{GS} = -0.1\,\text{V}$ & $V_{DS1} = 1\,\text{V}$).

NF takes a minimum value for $V_{DS1} \geq 0.8\,\text{V}$. The gain S_{21} takes the maximum value of 18 dB with $V_{DS1} = 1\,\text{V}$ and $1.2\,\text{V}$. Therefore, the optimal value of V_{DS1} in terms of NF, S_{21}, and P_{dc} is $1\,\text{V}$.

We can now fix $V_{GS} = -0.1\,\text{V}$ and $V_{DS1} = 1\,\text{V}$; then, we vary the voltage V_{DS2} of the second stage. The NF in Fig 7(a) is unchanged with the variation of V_{DS2}. The gain S_{21} is flat over the operating band; it is better for $V_{DS2} > 1.1\,\text{V}$, as shown in Fig. 7(b).

The compromise between minimum NF, high flat gain S_{21} and minimum P_{dc} imposes the bias of LNA as follows: $V_{GS} = -0.1\,\text{V}$, $V_{DS1} = 1\,\text{V}$ and $V_{DS2} = 1.1\,\text{V}$.

3.4. Effect of Resistors R_i on NF and S_{21} Gain

The parametric study of resistances R_i (i = 1, 2, 3, and 4) allows the design of a high performance LNA. The evolution of the input reflection coefficient S_{11}, the gain S_{21}, and the NF with respect to R_1 are shown in Fig. 8. R_1 is shunted at the input to adapt and extend the bandwidth of the LNA. According to Fig. 8(a), R_1 has an observational influence on S_{11} in the band [2 GHz–7 GHz]. Indeed, LNA is suitable for different values of $R_1 \geq 40\,\Omega$. The average NF minimum can be achieved with $R_1 = 80\,\Omega$, as shown in Fig. 8(b). The ripples at gain S_{21} are high for $R_i \leq 60$ Ohm. The optimum value of R_1 is 80 Ω.

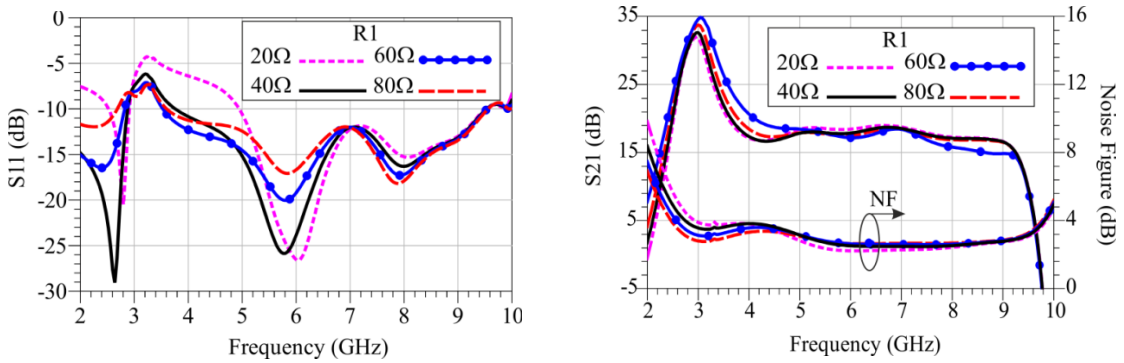

Figure 8. Influence of input matching resistance R_1 on: (a) Input reflexion coefficient, (b) forward gain S_{21} and NF.

We set $R_1 = 80\,\Omega$ and look for the optimal value of the inter-stage resistors R_2 and R_3. Figs. 9(a) and 9(b) show that R_2 and R_3 have an influence on the input reflection coefficients S_{11} and the output reflection coefficients S_{22} in particular on the higher frequency band. The NF of Fig. 9(c) varies slightly with R_2 and R_3. The gain S_{21} is reduced by 5 dB on the 3 GHz to 7 GHz band when R_2 and R_3 are set to 10 Ω and 40 Ω. For the value of 70 Ω, the gain is almost invariant. So, the optimum value of inter-stage resistors is 70 Ω.

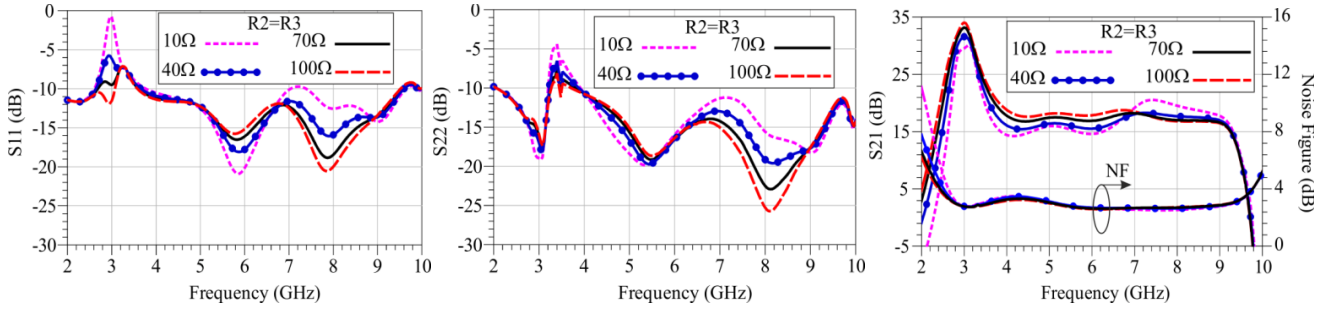

Figure 9. Influence of inter-stage resistors R_2 and R_3 on: (a) Input reflexion coefficient S_{11}, (b) output reflexion coefficient S_{22}, (c) forward gain S_{21} and NF.

The presence of the resistor R_4 allows the bandwidth to be extended. The output reflection coefficient S_{22} in Fig. 10(a) shows a better match for $R_4 \geq 35\,\Omega$. The variation of R_4 does not influence NF, as demonstrated in Fig. 10(b). The flat and maximum gain S_{21} is found for $R_4 = 35\,\Omega$.

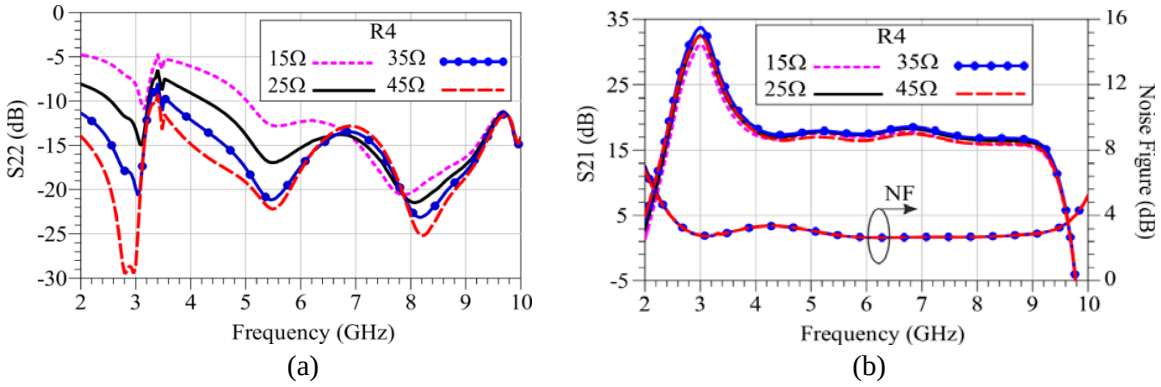

Figure 10. Influence of output matching resistance R_4 on: (a) output reflexion coefficient, (b) forward gain S_{21} and NF.

Finally, resistors $R_1 = 80\,\Omega$, $R_2 = 70\,\Omega$, $R_3 = 70\,\Omega$, and $R_4 = 35$ result in optimal noise figures and flat gain over a frequency band from 3.6 GHz to 9.5 GHz.

4. RESULTS AND DISCUSSIONS

Figure 11(a) shows the layout of a cascaded broadband LNA based on the resistive termination method. The layout is designed on planar technology based on an FR4 substrate. The layout area is small and occupies a chip size of $7\times1.3\,\text{cm}^2$. The copper part of the LNA layout is simulated with three-dimensional electromagnetic 3D-EM simulators of ADS. The EM simulation will be performed in 0 GHz to take into account the layout behaviour with the DC component, which will be used in the polarization of the transistors as well as the 2 GHz to 10 GHz band for the RF radiofrequency signal propagation. Then, we use co-simulation under ADS scheme to combine the extracted EM simulation result as S-parameters with the localized elements (R, L, C) and two MGF4918D transistors.

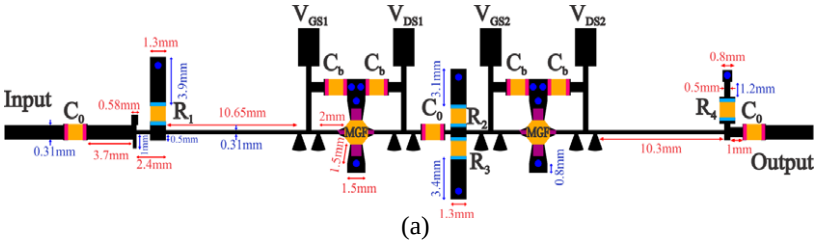

Figure 11. (a) Layout of cascade amplifier for broadband LNA and (b) picture of the LNA PCB.

To analyze the behaviour of LNA, all the ideal components are replaced by SMT (Surface Mount Technology) components from the AVX foundry, which has a tolerance of 1%.

Figure 11(b) shows a picture of the LNA chip. This chip is polarized by optimal tensions and connected with the VNA. LNA is measured over its entire operating frequency range [2 GHz–10 GHz]. To minimize the resulting errors in the measurement of the parameters $[S_{ij}]$, the number of points used

is 2001.

Figure 12 shows the results of measurements of K, μ_1, and μ_2 over a frequency range from 2 GHz to 10 GHz. The measured values are greater than 1, indicating that the designed LNA is unconditionally stable.

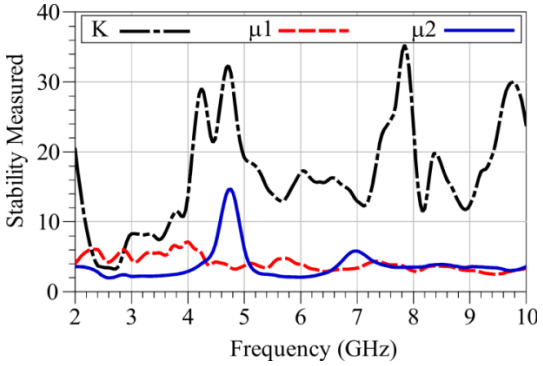

Figure 12. Measurements of Rollet factor K, stability factor for the source μ_1 and stability factor for the load μ_2 versus frequency.

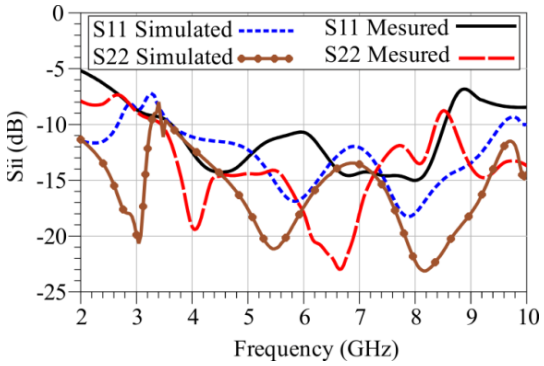

Figure 13. Input and output reflection coefficients versus frequency, comparison between simulation and measure.

The results of the measurement-simulation comparison of S_{11} and S_{22} of the two-stage LNA are generally excellent in the presence of the optimal R_i resistors and MLIN lines, as shown in Fig. 13. The measured S_{11} and S_{22} reflection coefficients are less than -10 dB in the 3.6 GHz to 8.5 GHz band; on the other hand, the EM simulation reaches up to 9.5 GHz. These results confer an excellent input and output match, and maximum power transfer takes place.

From Fig. 14(a), the average value of simulated gain S_{21} is 17.45 dB with a low ripple of 1.25 dB. The measured gain S_{21} is flat, and its value is equal to 14 ± 0.75 dB. Measurement errors (an increase in cable losses with frequency, limitation of frequency of the model of localized elements, the problem of soldering and SMA ports, ...) lead to a drop in the gain S_{21} of 3 dB. The cutoff frequency f_c of the LNA defines the bandwidth. This frequency decreases with increasing C_{gs} value. A small difference between the C_{gs} extracted from the electrical model (based on the datasheet) and the real component of the MGF transistor can lead to a small shift in the cutoff frequency in terms of simulation and measurement. The measurement and EM simulation results of the reverse gain S_{12} show the presence of perfect isolation between the output and input of LNA. In Fig. 14(b), the measured S_{12} of the LNA gives values ranging from approximately -50 dB to -30 dB.

Figure 15 shows the EM simulation results at both NF and $\mathrm{NF_{min}}$. $\mathrm{NF_{min}}$ agrees with NF over the

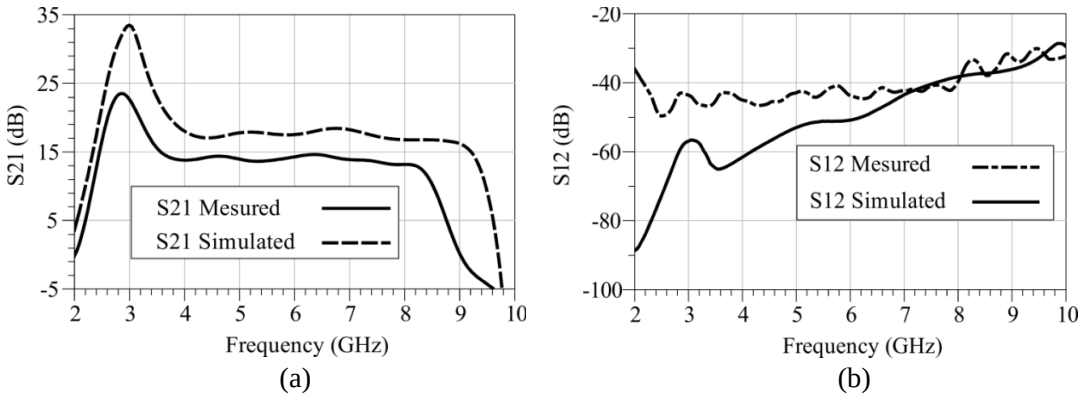

Figure 14. Simulation and measurement results of: (a) Forward gain S_{21} and (b) reverse isolation S_{12} of LNA.

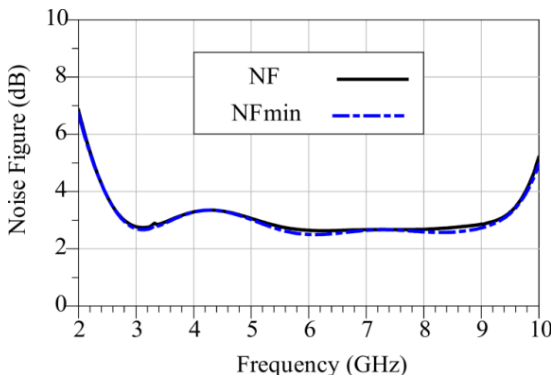

Figure 15. Noise figure co-simulation result.

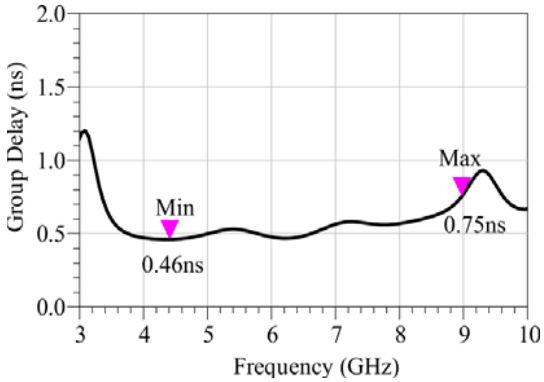

Figure 16. Group delay evolution of LNA.

bandwidth of interest and satisfies the low NF requirement at wideband. The noise figure of broadband LNA is 2.9 ± 0.4 dB. In Fig. 16, LNA achieves a group delay of 0.605 ± 0.145 ns. The GD value indicates that all RF signals, regardless of frequency, propagate from the input of the LNA to its load in the same time.

The power dissipation of the cascaded LNA is determined using the following formula:

$$P_{DC} = \sum_{i}^{n} V_{GSi} \cdot I_{GSi} + \sum_{i}^{n} V_{DSi} \cdot I_{DSi} \tag{11}$$

n is the number of stages used.

The LNA based on the MGF4918D transistor has a power dissipation of 164 mW.

The study of the nonlinear behaviour of LNA with the Harmonic Balance HB is used to determine the 1 dB compression point and third-order input intercept point IIP3. One-tone measurement for the 1 dB compression point was performed with VNA. Fig. 17 shows the evolution of the gain S_{21} with the input power P_{in} varying from -20 dBm to 25 dBm. The gain S_{21} is measured in three frequencies. The compression points measured at 5 GHz, 6 GHz, and 7 GHz are successively 11.8 dBm, 10.7 dBm, and 8 dBm. The $P_{1\,\mathrm{dB}}$ values show that LNA based on the InGaAs HEMT transistor has a perfect linearity.

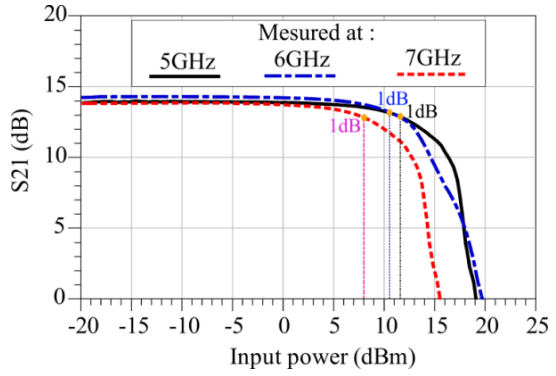

Figure 17. 1 dB compression point measurement.

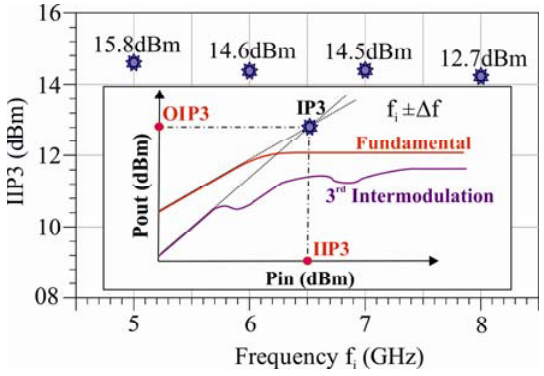

Figure 18. Co-simulation result of third-order input intercept point IIP3.

The point extrapolated from the linear sections of the fundamental frequency and third-order intermodulation frequency curves is given graphically as IP3. On the LNA, a two-tone test for third-order intercept was done. Two signals were applied at frequencies of $f_i - \Delta f$ and $f_i + \Delta f$ with $\Delta f = 5$ MHz. The results of IIP3 at frequencies f_i are shown in Fig. 18. IIP3 has a value of 14.25, 1.55 dBm.

Table 2 is a summary of the proposed broadband LNA and recently report state-of-the-art LNA design.

Table 2. Comparison of LNA performance with recent works.

Ref	**[26]$^{\Delta}$**	**[27]$^{\Delta}$**	**[28]$^{\Delta}$**	**This work**
year	2018	2019	2020	2022
Tech	GaN	GaN	GaAs-pHEMT	InGaAs-HEMT
Configuration	Cascode	Cascode	Cascaded	Cascaded
Number of stages	Two	Two	Three	Two
BW (GHz)	2.8–3.8	4.5–8	5–6	3.6–8.5
S_{11} (dB)	NA	NA	< -10	< -10
S_{22} (dB)	NA	NA	< -10	< -10
S_{12} (dB)	NA	NA	NA	< -30
S_{21} (dB)	13.5	11	34.3 ± 3.2	14 ± 0.75
NF (dB)	3	2.2 ± 0.8	0.59 ± 0.1	$2.9 \pm 0.4^{\Delta}$
Delay (ns)	NA	NA	NA	$0.605 \pm 0.145^{\Delta}$
$P_{1\,\mathrm{dB}}$ (dBm)	NA	NA	-16	10.16°
IIP3 (dBm)	25^{*}	NA	-4.1	$14.25 \pm 1.55^{\Delta}$
P_{dc} (mW)	2920	4500	417	164
Chip size (cm^2)	NA	NA	9.5×2	7×1.3
FOM	0.15	NA	17.98	21.23

$^{\circ}$ Average value $^{\Delta}$ Simulated * Value of OIP3

From the results shown in Table 2, which shows the comparison of LNA performance with recent works, we can conclude that the proposed LNA provides a low noise figure in comparison with [26]. The gain obtained is flat compared to [28] and greater than [26, 28]. The linearity of 14.25 dBm is favorable for broadband applications and better than [27]. The dissipated power of LNA in InGaAs technology is very low compared to GaAs and GaN [26–28] technologies. We can then say that broadband LNA offers the best FOM in terms of gain, noise, BW, power dissipation, and linearity.

5. CONCLUSION

In this paper, we have presented a two-stage planar cascaded broadband LNA based on a InGaAs HEMT transistor. A resistive termination technique is used to extend the bandwidth. A comparison of the designed LNA with the recent state-of-the-art shows that the proposed amplifier can provide excellent RF performance. Indeed, based on the results of the previous sections, we can conclude that over the frequency range of 3.6 to 8.5 GHz, the proposed broadband LNA exhibits high power gain, good input and output matching, low noise frequency, and excellent linearity.

REFERENCES

1. Le-Ngoc, T. and A. Masmoudi, *Full-duplex Wireless Communications Systems*, Springer International Publishing, Cham, 2017, https://doi.org/10.1007/978-3-319-57690-9.
2. Zhang, D., Z. Tian, and G. Wei, "Spatial capacity of narrowband vs. ultra-wideband cognitive radio systems," *IEEE Trans. Wirel. Commun.*, Vol. 7, 4670–4680, 2008, https://doi.org/10.1109/T-WC.2008.070746.

3. Zhu, J. and S. S. Kia, "UWB ranging aided pedestrian geolocation with GPB-based filtering for LoS and NLoS measurement processing," *2020 IEEE ION Position Locat. Navig. Symp. PLANS*, 781–787, IEEE, Portland, OR, USA, 2020, https://doi.org/10.1109/PLANS46316.2020.9110175.
4. Ling, R. W. C., A. Gupta, A. Vashistha, M. Sharma, and C. L. Law, "High precision UWB-IR indoor positioning system for IoT applications," *2018 IEEE 4th World Forum Internet Things WF-IoT*, 135–139, IEEE, Singapore, 2018, https://doi.org/10.1109/WF-IoT.2018.8355162.
5. Yin, Z., X. Jiang, Z. Yang, N. Zhao, and Y. Chen, "WUB-IP: A high-precision UWB positioning scheme for indoor multiuser applications," *IEEE Syst. J.*, Vol. 13, 279–288, 2019, https://doi.org/10.1109/JSYST.2017.2766690.
6. Poulose, A., O. S. Eyobu, M. Kim, and D. S. Han, "Localization error analysis of indoor positioning system based on UWB measurements," *2019 Elev. Int. Conf. Ubiquitous Future Netw. ICUFN*, 84–88, IEEE, Zagreb, Croatia, 2019, https://doi.org/10.1109/ICUFN.2019.8806041.
7. Kumar, A. R. A., A. Dutta, and B. D. Sahoo, "A low-power reconfigurable narrowband/wideband lna for cognitive radio-wireless sensor network," *IEEE Trans. Very Large Scale Integr. VLSI Syst.*, Vol. 28, 212–223, 2020, https://doi.org/10.1109/TVLSI.2019.2939708.
8. Xie, H., Y. J. Cheng, and Y. Fan, "A K-band high interference-rejection GaAs low-noise amplifier using multizero control method for satellite communication," *IEEE Microw. Wirel. Compon. Lett.*, Vol. 30, 1069–1072, 2020, https://doi.org/10.1109/LMWC.2020.3026075.
9. Kim, S. H. and Y. C. Rhee, "Implementation of Ku-band low noise block for global multi-band digital satellite broadcasting," *The Journal of the Korea Institute of Electronic Communication Sciences*, Vol. 11, 23–28, 2016.
10. Marimuthu, J., K. S. Bialkowski, and A. M. Abbosh, "Software-defined radar for medical imaging," *IEEE Trans. Microw. Theory Tech.*, 1–10, 2016, https://doi.org/10.1109/TMTT.2015.2511013.
11. Ha, H. K., "CMOS ultrasonic analogue front-end with reconfigurable pulser/switch for medical imaging applications," *Electronics Letters*, Vol. 51, No. 20, 1564–1566, 2015.
12. Stefigraf, I. and S. Rajaram, "Layout design of X-band low noise amplifier for radar applications," *International Symposium on VLSI Design and Test*, 140–156, Springer, Singapore, 2018, doi: 10.1007/978-981-13-5950-7_13.
13. Jeon, S.-Y., K. Nikitin, A. Dewantari, J. Kim, and M.-H. Ka, "Low-noise amplifier protection switch using p-i-n diodes with tunable open stubs for solid-state pulsed radar," *IEEE Microw. Wirel. Compon. Lett.*, Vol. 27, 1004–1006, 2017, https://doi.org/10.1109/LMWC.2017.2750029.
14. Feng, C., X. P. Yu, Z. H. Lu, W. M. Lim, and W. Q. Sui, "3–10 GHz self-biased resistive-feedback LNA with inductive source degeneration," *Electron. Lett.*, Vol. 49, 387–388, 2013, https://doi.org/10.1049/el.2012.4472.
15. Shim, Y., C.-W. Kim, J. Lee, and S.-G. Lee, "Design of full band UWB common-gate LNA," *IEEE Microw. Wirel. Compon. Lett.*, Vol. 17, 721–723, 2007, https://doi.org/10.1109/LMWC.2007.905633.
16. Kobayashi, K. W., D. Denninghoff, and D. Miller, "A novel 100 MHz–45 GHz input-termination-less distributed amplifier design with low-frequency low-noise and high linearity implemented with a 6 inch 0.15 mm GaN-SiC wafer process technology," *IEEE J. Solid-State Circuits*, Vol. 51, 2017–2026, 2016, https://doi.org/10.1109/JSSC.2016.2558488.
17. Fukui, H., "Optimal noise figure of microwave GaAs MESFE," *IEEE Transactions on Electron Devices*, Vol. 26, No. 7, 1032–1037, Jul. 1979, doi: 10.1109/T-ED.1979.19541.
18. Iversen, S., "The effect of feedback on noise figure," *Proc. IEEE*, Vol. 63, 540–542, 1975, https://doi.org/10.1109/PROC.1975.9784.
19. Friis, H. T., "Noise figures of radio receiver," *Proceedings of the IRE*, Vol. 32, 419–422, 1994, doi: 10.1109/JRPRO.1944.232049.
20. Rollett, J., "Stability and power-gain invariants of linear two ports," *IRE Trans. Circuit Theory*, Vol. 9, 29–32, 1962, https://doi.org/10.1109/TCT.1962.1086854.

21. Edwards, M. L. and J. H. Sinsky, "A new criterion for linear 2-port stability using a single geometrically derived parameter," *IEEE Trans. Microw. Theory Tech.*, Vol. 40, 2303–2311, 1992, https://doi.org/10.1109/22.179894.
22. Arekapudi, S., E. Iroaga, and B. Murmann, "A low-power distributed wide-band LNA in 0.18 µm CMOS," *2005 IEEE Int. Symp. Circuits Syst.*, 5055–5058, IEEE, Kobe, Japan, 2005, https://doi.org/10.1109/ISCAS.2005.1465770.
23. Ahn, K., R. Ishikawa, and K. Honjo, "Low noise group delay equalization technique for UWB InGaP/GaAs HBT LNA," *IEEE Microw. Wirel. Compon. Lett.*, Vol. 20, No. 7, 405–407, Jul. 2010, doi: 10.1109/LMWC.2010.2049441.
24. Park, Y., C. Lee, J. D. Cressler, and J. Laskar, "The analysis of UWB SiGe HBT LNA for its noise, linearity, and minimum group delay variation," *IEEE Trans. Microw. Theory Tech.*, Vol. 54, 1687–1697, 2006, https://doi.org/10.1109/TMTT.2006.872000.
25. Chen, M. and J. Lin, "A 0.1–20 GHz low-power self-biased resistive-feedback LNA in 90 nm digital CMOS," *IEEE Microw. Wirel. Compon. Lett.*, Vol. 19, 323–325, 2009, https://doi.org/10.1109/LMWC.2009.2017608.
26. Jarndal, A. H. and A. M. Bassal, "A broadband hybrid GaN cascode low noise amplifier for WiMax applications," *International Journal of RF and Microwave Computer-aided Engineering*, Vol. 2, 2018.
27. Jarndal, A., A. Hussein, G. Crupi, and A. Caddemi, "Reliable noise modeling of GaN HEMTs for designing low-noise amplifiers," *Int. J. Numer. Model. Electron. Netw. Devices Fields*, Vol. 33, 2020, https://doi.org/10.1002/jnm.2585.
28. El Bakkali, M., N. A. Touhami, and T.-E. Elhamadi, "High gain cascaded GaAs-pHEMT broadband planar low noise amplifier for WiMAX-80.16b application," *WITS*, 1101–1110, Springe, Singapore, 2022.